KSME

Springer

Journal of Mechanical Science and Technology 35 (11) 2021

Original Article
DOI 10.1007/s12206-021-1018-x

Keywords:
· CFD
· Design optimization
· Genetic algorithm
· Low-pressure axial-flow fan
· Stacking line
· Surrogate model

Correspondence to:
Tao Jin
cejintao@zju.edu.cn

Citation:
Kong, C., Wang, M., Jin, T., Liu, S. (2021). An optimization on the stacking line of low-pressure axial-flow fan using the surrogate-assistant optimization method. Journal of Mechanical Science and Technology 35 (11) (2021) 4997~5005. http://doi.org/10.1007/s12206-021-1018-x

Received December 21st, 2020
Revised July 20th, 2021
Accepted July 21st, 2021

† Recommended by Editor Yang Na

An optimization on the stacking line of low-pressure axial-flow fan using the surrogate-assistant optimization method

Chuang Kong[1], Meng Wang[1], Tao Jin[1] and Shaoliang Liu[2]

[1]College of Energy Engineering, Zhejiang University, Hangzhou 310058, China, [2]SuZhou Sigma Technology Co., LTD, Suzhou 215000, China

Abstract The shape of the blade stacking line greatly influences the low-pressure axial-flow fan's operational efficiency, but there is still no fast and effective way to determine the stacking line's optimal shape. This paper presents an automatic optimization design procedure for the blade stacking line in the low-pressure axial-flow fan based on the FINE/Design3D™ platform. The procedure combines computational fluid dynamics (CFD), surrogate model method, and genetic algorithm (GA) to execute a secondary optimization on a composite skewed-swept rotor-only axial fan blade. The results show that the static efficiency and the static pressure rise of the optimized fan respectively increase by 3.76 % and 5.82 % without stall margin decrease. The blade shape variation in skew and sweep direction reduces the tip leakage flow loss, improves the blade loading distribution, and contributes to the efficiency increment. This research provides a useful reference for the blade stacking line's automatic optimization for the axial-flow fan.

1. Introduction

As one of the essential industrial primary devices, low-pressure axial-flow fans are widely used in HVAC, cooling, ventilation, transportation, and other fields [1]. With improved social awareness on green energy conservation and cost-saving, axial-flow fans' design and optimization with high standards and strict requirements are critical [2]. Among the measures to improve the internal flow state and performance of the fan, the skewed-swept forming of blade stacking line has an important influence on the flow condition in blade channel [3], which leads to a widely studying and applying in the design and optimization of turbomachinery.

In a series of studies on the shape of the T35 low-pressure axial-flow fan impeller, Ouyanghua et al. [4] pointed out that the blade stacking line's circumferential skew can control the migration of tip leakage, improve the flow state in the tip area, and reduce tip leakage loss. In an optimization research of agriculture axial fan blade shape, Ding [5] found that the swept blade shape could alter the static pressure distribution on the blade surface and reduce the tip leakage flow. In particular, for transonic blades [6], a forward sweep blade cascade can decrease the load on the leading-edge (LE), while a backward sweep blade cascade can reduce the load on the trailing-edge (TE). However, there is still no consensus about the coupling effect of the composite skewed-swept blade stacking line on blade performance [7]. Besides, we still need to find a simple method to obtain the blade stacking line's optimal shape, matching with other shape parameters such as blade profile, installation angle, and chord length by changing the skew and the sweep of the blade.

With the rapid development of computer technology, the numerical optimization method combined with the computational fluid dynamics (CFD) technology has become an essential tool for the optimization design of turbomachinery, and it is widely used in the optimization design of turbomachinery, such as turbine [8, 9], compressor [10, 11] and pump [12, 13]. Therefore, this paper used the surrogate-assistant optimization technology and genetic algorithm to

Table 1. Main design parameters of the USI7.

Parameters	Value
Design flow rate q_v [m^3/s]	0.65
Rotational speed n [rev/min]	3000
Number of blades Z [-]	5
Hub diameter D_H [mm]	135
Shroud diameter D_S [mm]	300
Tip clearance [mm]	3

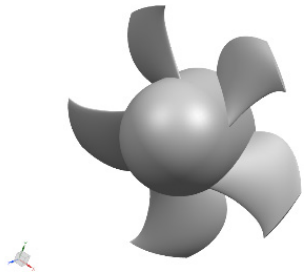

Fig. 1. The geometric model of USI7.

carry out the secondary optimization on a composite skewed-swept low-pressure axial-flow fan blade to explore the characteristics of the optimal stacking line shape. All work is finished on the Fine/Design3D™ rapid optimization design platform.

2. Simulation method

The baseline model is a rotor-only low-pressure axial fan USI7 designed based on blade element theory at the University of Siegen [14]. Its geometric model and test performance data were published by Carolus [15] in 2015. Fifteen NACA airfoils are stacked in the radial direction to form the blade, which has a skewed-swept shape considering noise reduction. The main design parameters and the geometric model are shown in Table 1 and Fig. 1.

The computational domain extends one diameter plane upstream and two diameter plane downstream from the impeller [16], as shown in Fig. 2. Only one blade channel is modeled in viewed of circumferential symmetry. The AutoGrid5™ is used to mesh the structured grid, and an O-type grid topology is applied near the blade region to improve the grid quality, as shown in Fig. 3. A low Reynolds number model *k-ω* SST [17] is selected to solve the steady-state RANS equation. Thus, the y$^+$, which close to solid walls, is defined as 1. The boundary conditions are set as follows: a mass flow rate boundary condition and a static pressure boundary condition are applied to inlet and outlet, respectively; no sliding wall boundary condition is adopted for solid walls, and the hub and blade rotate at a speed of 3000 rpm while the shroud remains stationary. The convergence criteria of the simulation is global residual < 1e-6.

Several grid sets are selected for simulation analysis to eliminate the numerical error introduced by grid density difference. Fig. 4 shows the variation of fan total-static pressure rise

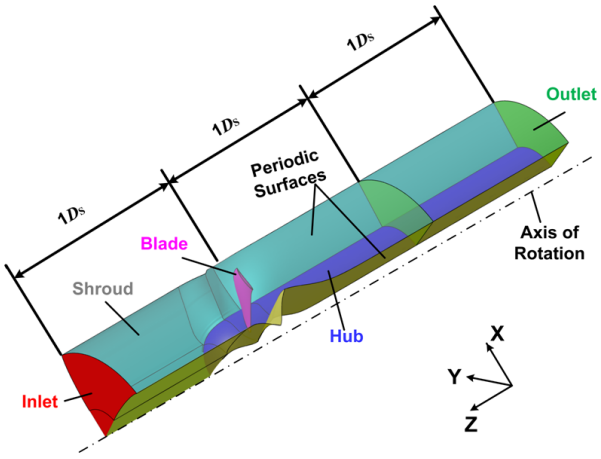

Fig. 2. Computational domain.

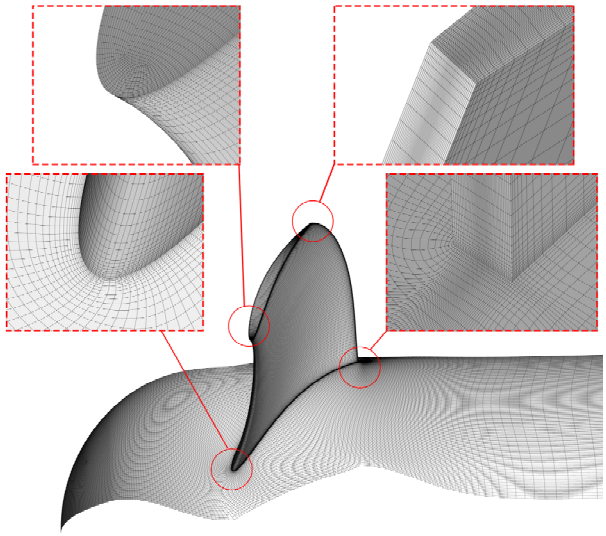

Fig. 3. Meshing grid details of USI7.

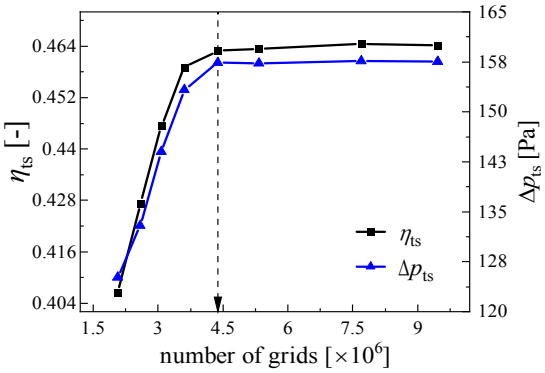

Fig. 4. Verification of mesh independence.

and total-static efficiency vs. the number of grid nodes, which is finally determined to be 4.38×10^6 considering the calculation cost and validity.

According to the above simulation conditions and mesh settings, the fan performance under different flow conditions is

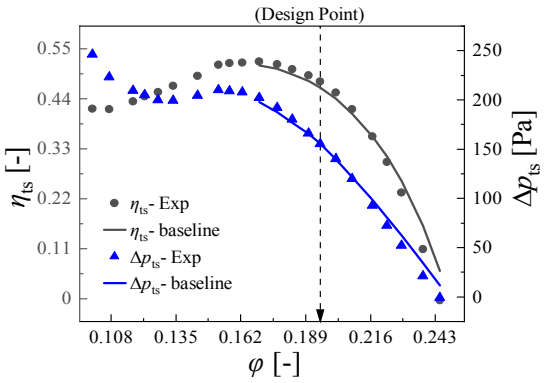

Fig. 5. Comparison of simulation results and experiment results.

simulated and compared with the published test data [15], which can be seen in Fig. 5. Eqs. (1)-(3) present the definitions of total-static pressure rise, total-static efficiency, and axial fan flow coefficient, where p_{2s} is the static pressure at the outlet, p_{1t} is the total pressure at the inlet, q_v is the volume flow rate, P_{Shaft} is the shaft power, and D is the blade tip diameter. Under the design operating condition (φ = 0.195), the simulation results are highly consistent with the fan's real performance, proving that the CFD simulation results can be used as the basis for the blade shape optimization and improvement.

$$\Delta p_{ts} = p_{2s} - p_{1t} \tag{1}$$

$$\eta_{ts} = \frac{q_v \Delta p_{ts}}{P_{Shaft}} \tag{2}$$

$$\varphi = \frac{4q_v}{\pi^2 D^3 n}. \tag{3}$$

3. Optimization flow

To increase optimization efficiency, a surrogate-assistant automatic stacking line optimization flow is built based on the FINE/Design3D™ platform, Fig. 6. The CFD simulation process has been introduced in the upper section, and the rest parts of the optimization flow are described below.

In order to facilitate blade geometric modeling and parametrization, we adopt the blade sweep and skew definitions in references [18-20]. In the first place, the stacking line is circular and planar projected onto the meridional plane and the axial plane, respectively. The circular lean of the stacking line on the axial plane is defined as skew, and the axial lean of the stacking line on the meridional plane is defined as sweep, as shown in Fig. 7.

A third-order Bézier curve [21] is applied to fit the skew feature and sweep feature of the stacking line, considering its good graphics intuition and continuity, and four control points P0, P1, P2, and P3 are obtained on each plane. The end control point P0 is fixed on the hub as the anchor point, through which a radial line is made and set as the reference line for the stacking line. Finally, the remaining three control points are

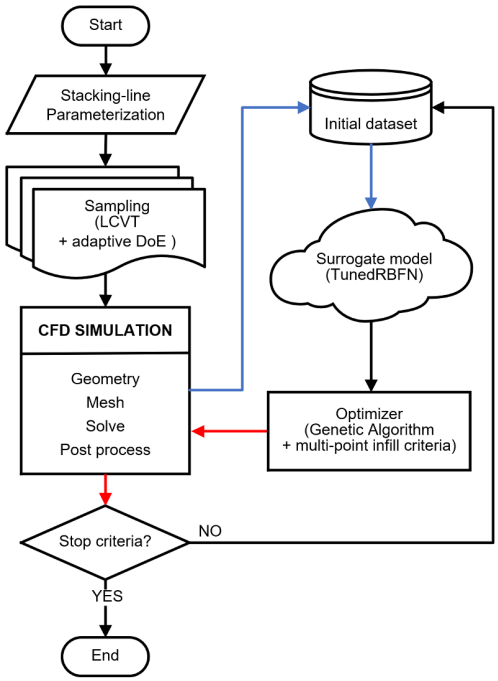

Fig. 6. Axial fan stacking-line optimization flow chart.

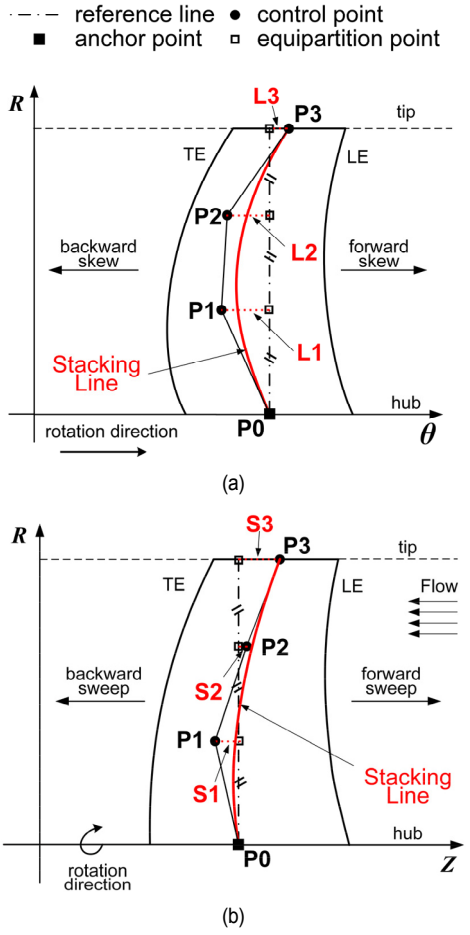

Fig. 7. Parametric definition of the skewed-swept stacking line based on the Bézier curve: (a) skew in the axial plane; (b) sweep in the meridian plane.

Table 2. Initial values and upper and lower limits of the design variables.

Design variables	Lower limits	Values of reference model	Upper limits
S1	-0.3	-0.0673	0.1
S2	-0.2	-0.0304	0.3
S3	-0.1	0.0784	0.4
L1	-0.3	-0.1418	0.1
L2	-0.2	-0.0637	0.6
L3	-0.1	0.1414	0.3

uniformly distributed along the radial direction, and the distances between the control points and the radial reference line are defined as the design parameters, namely (L1, L2, L3) for the skew and (S1, S2, S3) for the sweep. The corresponding initial values and the upper and lower limits of design variables are listed in Table 2. Meanwhile, the axial fan's total-static efficiency under the design condition is selected as the objective function considering the research target and computational expense. To maintain the stall margin of the fan, the total-static pressure rise near the stall point (φ = 0.169) is selected as a constrain, which is handled by the constraint tournament selection method [22] during the optimization.

Next, two sampling steps are taken to build the surrogate model, which is used to fit the system input and response relationship. First, the latinized centroidal Voronoi tessellations (LCVT) method [23] is used to draw 100 samples within six design variables to form the initial dataset. The LCVT can effectively produce a highly uniform distribution of sample points over the parameter spaces. The CFD method is applied to simulate each sample point to acquire the corresponding response. Furthermore, the relationships between every stacking line design parameter and the objective & constrain function are fitted by the tuned radial basis functions (TunedRBF) method [24], which does not need to prescribe the type of basis function and hyper-parameter values compared to the classical RBF model. In the training process, the radial basis functions of the TunedRBF are selected between Gaussian and multiquadric, and the hyper-parameter values are adjusted automatically, utilizing the heuristic based on the correlation coefficient of the model [25], which is calculated by Leave-One-Out method [26]. Second, another 53 samples are drawn using an adaptive DOE technique, which iteratively refines the sample dataset where the model response exhibits its maximum of error, with the error indicator based on the cross-validation LOO procedure.

Finally, the genetic algorithm (GA) is utilized to search the surrogate model's optimum, while the population size, the number of generations, and the GA's mutation probability are set as 400, 100, and 0.01, respectively. After getting the current surrogate model's optimum, a CFD computation for the optimum sample point is carried out to verify whether the stop criteria are satisfied. If the condition of convergence is fulfilled, the optimization loop is over. Otherwise, the sample has to be

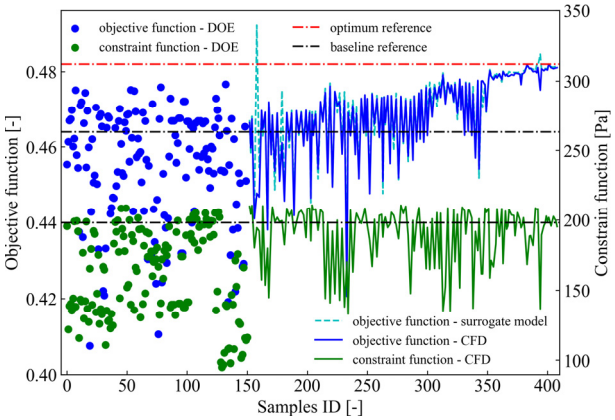

Fig. 8. Samples history during the optimization.

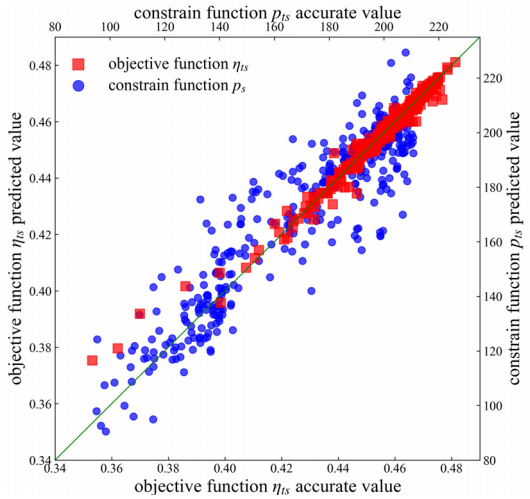

Fig. 9. Global correlation coefficient of η_{ts} (0.987) and p_s (0.926) based on LOO cross-validation analysis.

added to the initial data set to reconstruct the surrogate model. The GA searching process repeats until the optimum is acquired. To avoid the optimal search gets stuck at a local optimum, a multi-point infill criteria named feasibility strategy [27-29] is adopted for this constrained optimization problem. During the GA process on the surrogate model, 10 individuals of high feasibility are stored and updated at each generation and outer design iteration. Then, 2 points are chosen among all the stored points according to the global objective and the distance to existing points, and added to the database along the "best" point found by the optimization on the surrogate model.

The optimization calculation is executed on a high-performance computing platform, whose CPU is Intel Xeon E5 2680 v4 with 2.4 GHz clock frequency. It takes 135 hours on 128 processors to finish the entire optimization process, during which 410 samples are simulated by CFD. As shown in Fig. 8, the sampling stage totally generates 153 samples and the optimization stage generates 257 samples. The optimum is achieved at the 252th iteration. The global correlation coefficient

Table 3. The performance parameters of the baseline and the optimized fan under design condition.

Parameters	Baseline impeller	Optimized impeller	Improvement
Total-static efficiency η_{ts} [-]	0.464	0.482	3.76 %
Total-static pressure rise Δp_{ts} [Pa]	155.3	164.3	5.82 %

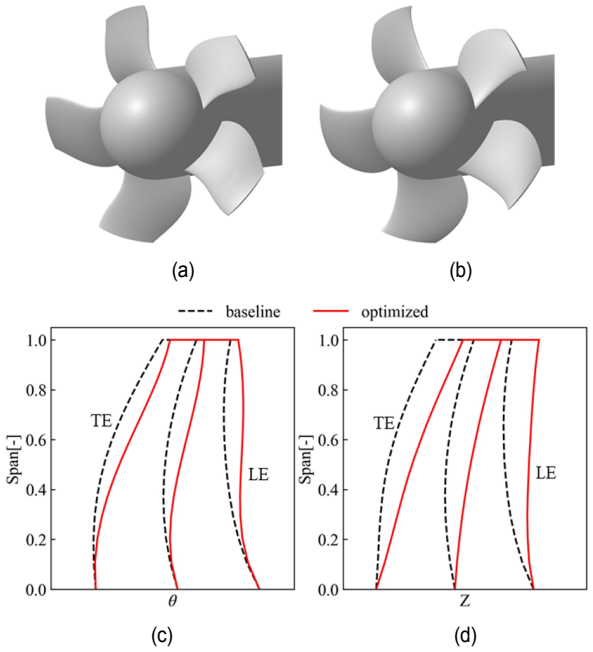

Fig. 10. Comparison of geometry and stacking line between the baseline and the optimized: (a) the optimized fan geometry; (b) the baseline fan geometry; (c) the axial plane; (d) the meridional plane.

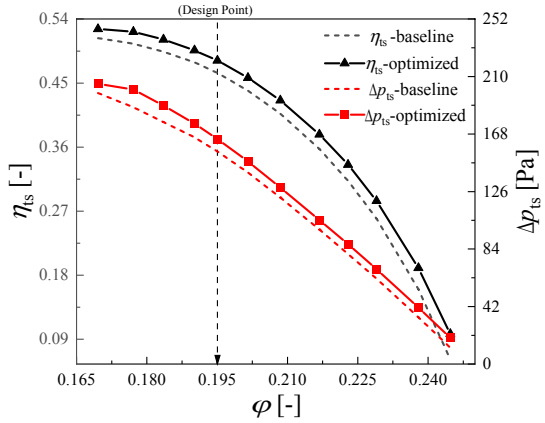

Fig. 11. Aerodynamic performance curves of the baseline and the optimized fan.

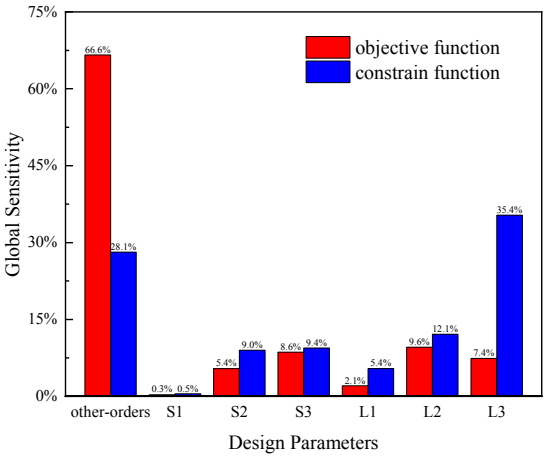

Fig. 12. The sensitivity of the objective and constrain function to design variables.

of the objective function and the constraint function are analyzed by LOO cross-validation method after the optimization, as shown in Fig. 9 that the correlation coefficient is 0.987 for η_{ts} and 0.926 for p_s, which means that the TunedRBF is of high accuracy and the optimization results are credible.

3.1 Results

After the optimization, the status of the design variables is {S1 = 0.0238, S2 = 0.1000, S3 = 0.1868, L1 = -0.1407, L2 = 0.1700, L3 = 0.1890}. We compared the variation of blade shape and the stacking line with the baseline, as shown in Fig. 10. The skew feature in Fig. 10(c) becomes from the backward-forward skew to the slightly-backward and forward-straight skew, and the shape of the stacking line becomes from the "C" to the retrography "S". While, the sweep feature in Fig. 10(d) becomes from the backward-forward sweep to the pure forward sweep.

Table 3 lists the performance comparison between the baseline and the optimized axial fan under the design condition ($\varphi = 0.195$). The static efficiency of the optimized impeller increases by 3.76 %, while the static pressure of the optimized impeller increases by 5.82 %. The operation performance of the fan under stable working conditions is simulated to comprehensively display the optimization effects. The results are presented in Fig. 11. The overall static efficiency and static pressure of the optimized fan are significantly improved compared with the baseline. Due to the pressure rise constrain near the stall point, the fan stability margin has been retained.

To compare the noise performance variation of the fan before and after the optimization, the aero-acoustic simulations are carried out using the CFX and Actran software [30]. The sound pressure level is monitored at the upstream location. The maximum noise value for the baseline and the optimized are 54.03 dB and 53.52 dB, respectively, which means the optimized fan is 0.51 dB quieter than the baseline.

To explore the influence of design variables on the objective and constrain function, the global sensitivities are evaluated by

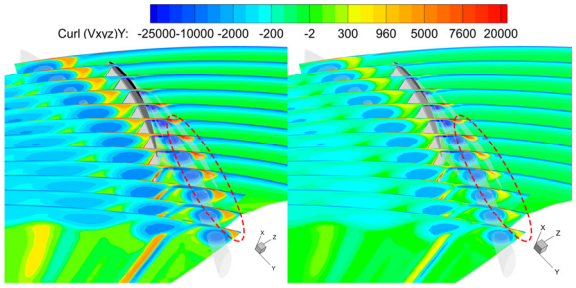

Fig. 13. The y-component contour of the vorticity and the tip leakage vortex(Q = 5e6) at the blade tip region: (a) baseline; (b) optimized.

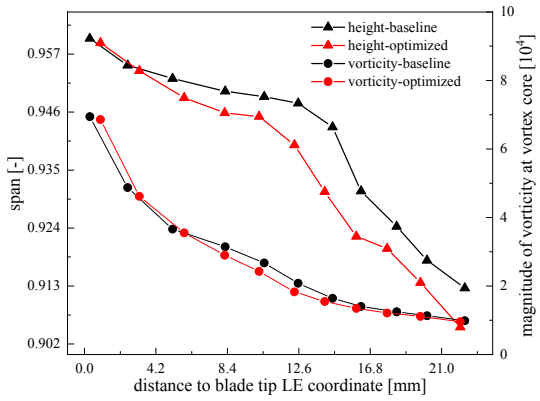

Fig. 14. Radial height and vorticity of the vortex core trajectory.

the sobol′ method [31] based on the TunedRBFN model. Fig. 12 presents the impact index of different parameters on the response functions. For the objective function, the influence of other-order takes up as high as 66.6 %, which means the interaction among design parameters has a conclusive influence on the improvement of static efficiency. For the constrain function, the L3 (tip skew) and other-order have the greatest influences on the stall margin. In general, during the optimization, interaction among design parameters is very important, and the tip skew should be paid more attention.

4. Discussion

To explore the influence of blade tip skew angle changing on the fan's flow condition, tip leakage vortex's structure and strength are compared between the optimized and the baseline. As shown in Fig. 13, the tip leakage vortex structure is identified by the Q criterion [32], and the tip leakage vortex strength is identified by the Y-component of the velocity curl contour. The tip leakage vortex's optimized structure is similar to the baseline, but the secondary vortex intensity is reduced, which means tip leakage loss is reduced, and static efficiency is improved. The vortex core trajectory and the vorticity of the tip leakage vortex is plotted based on the method in Ref. [33]. As shown in Fig. 14, the X-axis is defined as the distance between the tip vortex core and the blade tip leading edge point. In the

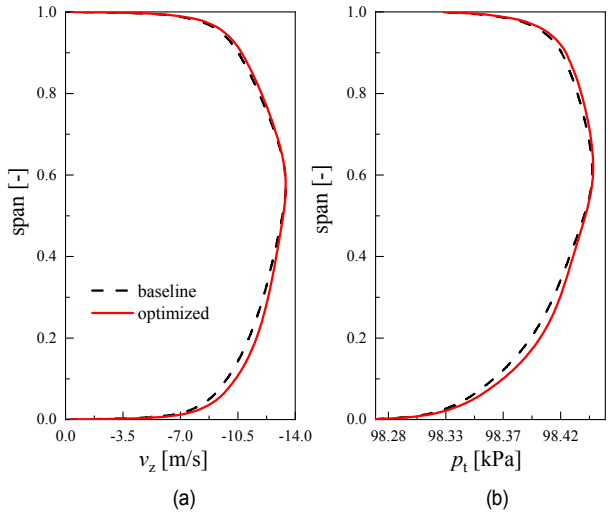

Fig. 15. The circumferential averaged axial velocity (a); total pressure (b) at the outlet.

middle area of the optimized blade passage, the magnitude of vorticity at vortex core is smaller than the baseline, and the radial height of the vortex core in the downstream area is significantly lower than the baseline, indicating a rapid dissipation of the vortex. This process weakens the influence on subsequent flows and contributes to the improvement of fan efficiency.

Fig. 15 shows the distribution of circumferential averaged axial velocity and total pressure along the outlet's spanwise direction. In span range 0.05-0.5 and 0.65-0.95, the average axial velocity and average pressure are both increased, indicating the work ability of the fan is enhanced, which is conducive to improving the static efficiency.

To further demonstrate the influence of stacking line changes on the blade's work capacity, the static pressure difference between the pressure surface and the suction surface is defined as the blade load. Fig. 16 shows the distribution of blade surface static pressure and blade load at the different spanwise locations. In an area of 0-0.8 span, the static pressure on the pressure surface of the optimized blade remains unchanged, but the decrease of the static pressure on the suction surface leads to increased blade load, which means an increasement in the ability of doing work. The static pressure near pressure side leading-edge goes up in 0.85 and 0.9 span, while there are regional differences in the static pressure on the suction surface. As shown in Figs. 16(e) and (f), in the suction surface area, the static pressure near leading-edge starts to decrease at about 0.9 span, while the static pressure near trailing-edge starts to increase at about 0.95 span. This means the load near the blade leading edge decreases and near the blade trailing edge increases. The main reason for the different load distribution is that the degree of forward-skew and forward-sweep at the tip area of the optimized blade stacking line has increased, leading to a change of tip leakage vortex strength, and affecting the blade load distribution.

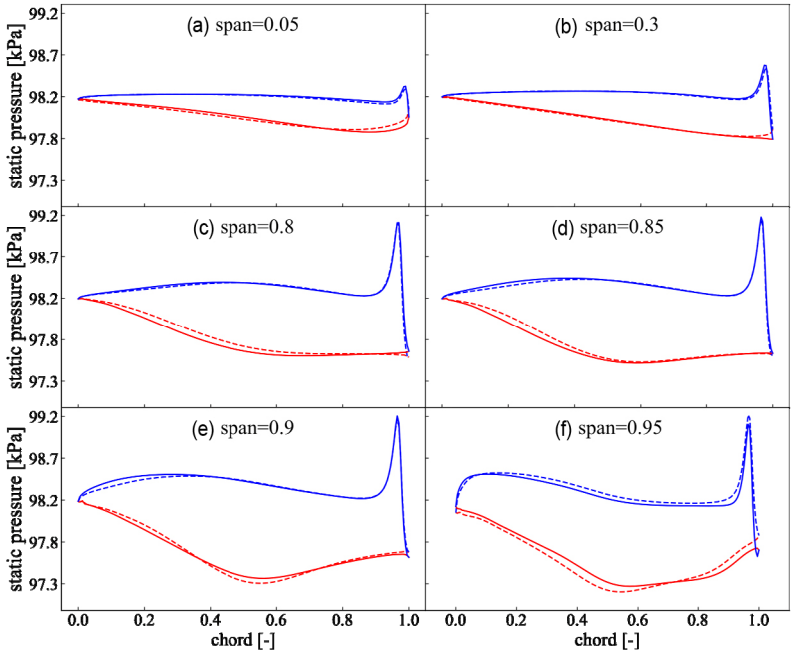

Fig. 16. Static pressure distribution at different spans (Dash line: Baseline, Line: Optimized, Red: Suction side, Blue: Pressure side).

5. Conclusions

Based on the FINE/Design3D™ platform, this paper systematically proposed an automatic design and optimization method for the shape of the blade stacking line, whose objective function is static efficiency. Furthermore, in combination with CFD technology, surrogate model, and numerical optimization method, as well as a Bézier curve for the use of stacking line parameterization, this method obtained good optimization results, which provides a useful reference for the design of blade stacking line of a low-pressure axial-flow fan.

1) By using the automatic optimization design method to optimize the existing fan, the new shape of the stacking line changed significantly in the skew and sweep direction: The skew feature becomes from the backward-forward skew to the slightly-backward and forward-straight skew, and the shape of the stacking line becomes from the "C" to the retrography "S". While, the sweep feature becomes from the backward-forward sweep to the pure forward sweep. The forward degree of the skew and sweep are both enhanced than the baseline, which resulted in the increase of the load of the upper blade height area and the improvement of the work capacity. Under the design condition, the optimized fan's static efficiency and static pressure increased by 3.76 % and 5.82 %, respectively. In stable operating conditions, the static pressure rise and static efficiency are significantly improved as well.

2) We analyze the influence of blade tip skew characteristics on the flow state inside the fan for its more significant influence on the static efficiency. The results show that: in a region smaller than 0.8 span, the static pressure decreases on the suction surface, and the average axial velocity and average pressure at the outlet increase within a range smaller than 0.5 span and greater than 0.65 span, indicating that flow near the tip and corner area of the blade is improved, and the power capacity is promoted. Moreover, the tip leakage loss is reduced, and static efficiency is improved after the optimization.

Prospect: This paper only optimizes a single efficiency target, but the shape of a stacking line also significantly impacts noise performance. Though the optimized fan slightly improves the noise performance of the baseline in this study, it is still hoped that the multi-objective collaborative optimization of efficiency and noise can be considered in future studies.

Acknowledgments

The authors would like to acknowledge Thomas H. Carolus for his generous provision of geometry and testing data about USI7. The computational resource was supported by the HPC center of ZJU (ZHOUSHAN CAMPUS).

Nomenclature

CFD	: Computational fluid dynamics
DoE	: Design of experiments
GA	: Genetic algorithm
LCVT	: Latinized centroidal voronoi tessellations
LE	: Leading-edge
RBF	: Radial basis functions
TE	: Trailing-edge
n	: Rotational speed
p_{1t}	: Total pressure at the inlet
p_{2s}	: Static pressure at the outlet
p_t	: Total pressure
Δp_{ts}	: Total to static pressure rise

q_v : Volume flow rate
v_z : Axial velocity
D : Blade tip diameter
D_H : Hub diameter
D_S : Shroud diameter
P_{Shaft} : Shaft power
Z : Number of blades
η_{ts} : Total to static efficiency
φ : Flow coefficient

References

[1] J. Li et al., Aerodynamic design and optimization of a high-loaded axial fan stage using a curvature control method, *J. Mech. Sci. Technol.*, 33 (8) (2019) 3871-3883.

[2] S. Heo et al., Development of high-performance and low-noise axial-flow fan units in their local operating region, *J. Mech. Sci. Technol.*, 29 (9) (2015) 3653-3662.

[3] Z. Wang and Y. Zheng, Research status ans development of the bowed-twisted blade for turbomachines, *Engineering Science*, 2 (6) (2000) 40-48.

[4] H. Ouyang et al., Experimental study on aerodynamic and aeroacoustic performance of low pressure flow fan with circumferential skewed blades, *Journal of Aerospace Power*, 21 (4) (2006) 668-674.

[5] T. Ding et al., Optimization design of agricultural fans based on skewed-swept blade technology, *Applied Engineering in Agriculture*, 35 (2) (2019) 249-258.

[6] P. Song and J. Sun, Blade shape optimization for transonic axial flow fan, *J. Mech. Sci. Technol.*, 29 (3) (2015) 931-938.

[7] S. J. Seo, S. M. Choi and K. Y. Kim, Design optimization of a low-speed fan blade with sweep and lean, *Proceedings of the Institution of Mechanical Engineers, Part A: Journal of Power and Energy*, 222 (1) (2008) 87-92.

[8] S. S. Talya, A. Chattopadhyay and J. N. Rajadas, Multidisciplinary design optimization procedure for improved design of a cooled gas turbine blade, *Engineering Optimization*, 34 (2) (2002) 175-194.

[9] J.-H. Jeong and S.-H. Kim, Optimization of thick wind turbine airfoils using a genetic algorithm, *J. Mech. Sci. Technol.*, 32 (7) (2018) 3191-3199.

[10] J. Li, Q.-H. Deng and Z.-P. Feng, Multiobjective optimization design of a compressor airfoil using evolutionary algorithms, *Proceedings of the Chinese Society of Electrical Engineering*, 24 (10) (2004) 205-209.

[11] S. Pierret, R. F. Coelho and H. Kato, Multidisciplinary and multiple operating points shape optimization of three-dimensional compressor blades, *Structural and Multidisciplinary Optimization*, 33 (1) (2007) 61-70.

[12] M.-W. Heo et al., High-efficiency design of a mixed-flow pump using a surrogate model, *Journal of Mechanical Science and Technology*, 30 (2) (2016) 541-547.

[13] M.-W. Heo et al., High-efficiency design optimization of a centrifugal pump, *J. Mech. Sci. Technol.*, 30 (9) (2016) 3917-3927.

[14] T. H. Carolus and R. Starzmann, An aerodynamic design methodology for low pressure axial fans with integrated airfoil polar prediction, *American Society of Mechanical Engineers Digital Collection* (2012) 335-342.

[15] T. Carolus, T. Zhu and M. Sturm, A low pressure axial fan for benchmarking prediction methods for aerodynamic performance and sound, *Noise Control Engineering Journal*, 63 (6) (2015) 537-545.

[16] T. Zhu and T. H. Carolus, Axial fan tip clearance noise: experiments, Lattice-Boltzmann simulation, and mitigation measures, *International Journal of Aeroacoustics*, 17 (1-2) (2018) 159-183.

[17] F. R. Menter, Two-equation eddy-viscosity turbulence models for engineering applications, *AIAA Journal*, 32 (8) (1994) 1598-1605.

[18] M. G. Beiler and T. H. Carolus, Computation and measurement of the flow in axial flow fans with skewed blades, *Journal of Turbomachinery*, 121 (1) (1999) 59-66.

[19] M. Masi and A. Lazzaretto, A simplified theory to justify forward sweep in low hub-to-tip ratio axial fan, ASME turbo expo: turbine technical conference and exposition, *Amer. Soc. Mechanical Engineers*, New York, 1 (2015) V001T09A011.

[20] J. Vad, Forward blade sweep applied to low-speed axial fan rotors of controlled vortex design: an overview, *J. Eng. Gas. Turbines Power-Trans. ASME*, 135 (1) (2013) 012601.

[21] K.-S. Lee, K.-Y. Kim and A. Samad, Design optimization of low-speed axial flow fan blade with three-dimensional RANS analysis, *J. Mech. Sci. Technol.*, 22 (10) (2008) 1864-1869.

[22] K. Deb, An efficient constraint handling method for genetic algorithms, *Computer Methods in Applied Mechanics and Engineering*, 186 (2-4) (2000) 311-338.

[23] Y. Saka, M. Gunzburger and J. Burkardt, Latinized, improved LHS, and CVT point sets in hypercubes, *International Journal of Numerical Analysis and Modeling*, 4 (3-4) (2007) 729-743.

[24] C. M. Bishop, *Neural Networks for Pattern Recognition*, Oxford University Press (1995).

[25] C. Sainvitu, V. Iliopoulou and I. Lepot, *Global Optimization with Expensive Functions - Sample Turbomachinery Design Application*, M. Diehl, F. Glineur, E. Jarlebring, W. Michiels (Eds.), Recent advances in optimization and its applications in engineering, Springer, Berlin, Heidelberg (2010) 499-509.

[26] S. Rippa, An algorithm for selecting a good value for the parameter c in radial basis function interpolation, *Advances in Computational Mathematics*, 11 (2) (1999) 193-210.

[27] C. Beauthier, P. Beaucaire and C. Sainvitu, A surrogate-based evolutionary algorithm for highly constrained design problems, *Proceedings of the Genetic and Evolutionary Computation Conference Companion, ACM*, Berlin, Germany (2017) 1613-1613.

[28] P. Beaucaire, C. Beauthier and C. Sainvitu, Exploitation of multiple surrogate models in multi-point infill sampling strategies, *Proceedings of the Genetic and Evolutionary Computation Conference Companion, Association for Computing Machinery*, New York, USA (2019) 245-246.

[29] P. Beaucaire, C. Beauthier and C. Sainvitu, Multi-point infill

sampling strategies exploiting multiple surrogate models, *Proceedings of the Genetic and Evolutionary Computation Conference Companion, Association for Computing Machinery*, New York, USA (2019) 1559-1567.

[30] Free Field Technologies SA, *ACTRAN 2020 User's Guide* (2019).

[31] I. M. Sobol′, Global sensitivity indices for nonlinear mathematical models and their Monte Carlo estimates, *Mathematics and Computers in Simulation*, 55 (1) (2001) 271-280.

[32] J. C. Hunt, A. A. Wray and P. Moin, *Eddies, Streams, and Convergence Zones in Turbulent Flows*, *NASA Ames Research Center*, Stanford University (1988).

[33] G. Jin, H. Ouyang and Z. Du, Numericla analysis on tip leakage flow of circumferential skewed blades according to flow rates, *Journal of Aerospace Power*, 24 (9) (2009) 2107-2114.

Chuang Kong is currently a Ph.D. candidate in the Institute of Process Equipment, College of Energy Engineering, Zhejiang University, China. He received his B.S. degree from Dalian University of Technology, China, in 2016. His research interests include computational fluid dynamics and design optimization of turbomachinery.

Tao Jin is currently a Professor at Zhejiang University, China. He received his B.S. degree from Zhejiang University, in 1985, and his M.S. and Ph.D. in the Department of Chemical Engineering from the same university in 1989 and 2000, respectively. His research interests include fluid-machinery, computational aided design, and computational aided engineering.